2nd URSI AT-RASC, Gran Canaria, 28 May – 1 June 2018

A Bottomside Profile Function for the Empirical Canadian High Arctic Ionospheric Model (E-CHAIM)

David R. Themens[(1)], and P.T. Jayachandran [(1)]
(1) Department of Physics, University of New Brunswick, Fredericton, NB, Canada

Abstract

Following the development of the Empirical Canadian High Arctic Ionospheric Model (E-CHAIM)'s F2-peak and topside components, we have now undertaken the challenge of creating a matching bottomside for E-CHAIM. For this bottomside, we have developed a variable semi-Epstein layer parameterization, where the scale thicknesses of this layer are represented by a sum of layer functions associated with the E-region, F1-layer, and F2-layer. The coefficients of each of these layers are independently modeled using a spherical cap harmonic expansion in magnetic latitude and magnetic local time to represent horizontal and diurnal variability. A Fourier expansion in day of year is used to represent seasonal variations. By modeling our bottomside in the scale thickness domain of a single layer, we avoid the need for an F1-layer occurrence trigger, such as that used by the International Reference Ionosphere (IRI).

This study details the E-CHAIM bottomside profiler, whose development was informed by challenges that have been reported in the use of the IRI and NeQuick.

1. Introduction

The bottomside of E-CHAIM is, perhaps, the most challenging component of the model. The bottomside is highly vertically structured and consists of layers with very different or independent physical dynamics. This difference in the behaviour of the ionosphere's various bottomside layers and the tendency of some of these layers to only exist part of the time (F1-layer/ledge and E-region) necessitates that one takes separate considerations for each of these regions.

In light of this challenge, one would be tempted to attempt to re-fit current standards like the IRI and NeQuick; however, each of these formulations have been found to exhibit undesirable behaviour that we here wish to avoid.

2.1 Current Standards: IRI

The IRI bottomside is composed of five sub-regions: the F2-region, the F1-region, an Intermediate region between the F1-region and the E-F valley, an E-F valley region, and a lower E-region/D-region [Bilitza, 2003; and Reinisch and Huang, 2000]. Their decomposition of the bottomside is very complex and was designed to be flexible enough to accommodate the modeling of the bottomside globally, where different geographic locations demonstrate vastly different bottomside behaviour.

Each of the five bottomside regions is modeled using the same layer function as the F2-region but with separate modified height terms that are dependent of hmF1 and hmE. In this way, the IRI bottomside is essentially a piece-wise continuous function with equal densities forced at the boundary of each region. This piece-wise parametrization of the bottomside acts as a somewhat severe limitation of the IRI bottomside, as the vertical gradient of the electron density at the boundary of each region is not continuous despite the electron density itself being continuous. This poses significant challenges for users interested in ray tracing, as such applications require that the electron density profile has a continuous derivative.

hmE, the height of the E-region peak, in the IRI is taken as a constant value of 105km. For the altitude of the F1-region peak, the IRI simply uses the altitude at which their F2-region profile reaches the density corresponding to their modelled foF1.

Because of the intermittent occurrence of the F1-region, the occurrence model of Scotto et al. [1998] is used to determine when to include the F1-layer/ledge. This trigger can lead to discontinuous spatial variations in electron density in the transition between regions with and without an F1-layer. If an F1-region is determined to be present, the electron density in the region of the F1-layer/ledge is given by the same function as the F2 bottomside, but with a modified height term given in Bilitza [2003].

2.2 Current Standards: NeQuick

The NeQuick bottomside is given as the sum of three semi-Epstein layer functions, each with different topside and bottomside scale thicknesses. The NeQuick uses the foF1 model of Leitinger et al. [2005] for its foF1, which parameterizes foF1 as a piece-wise function of foE. foE in the NeQuick is then modeled using the work of Titheridge [1996]. hmE in the NeQuick is taken as a constant value of 120km and hmF1 is set as the average of hmF2 and hmE.

Unlike the IRI, the NeQuick bottomside model has a continuous vertical gradient profile, despite using discontinuous thickness changes at the layer peaks. This continuity is guaranteed, despite the thickness changes at each layer peak, because the derivative is zero at the peak

by construction (a property of a semi-Epstein layer function), regardless of the thickness. This gives the NeQuick an advantage over the IRI when one wishes to use the model for HF ray tracing

3. E-CHAIM

For the bottomside portion of the E-CHAIM model, we make use of global ionosonde profiles from the Global Ionosonde Radio Observatory (GIRO) and the Canadian High Arctic Ionospheric Network (CHAIN). We are here restricted to a substantially smaller dataset than what was available for the NmF2 and hmF2 portions of the model for a number of reasons, as many of the older datasets did not invert electron density profiles from their data, instead scaling only foF2, MUF(3000)F2, and foE. In addition to this, the bottomside electron density profile, as a whole, is quite sensitive to scaling errors; thus, in addition to the quality control measures used for the hmF2 portion of the model, described in Themens et al. [2017], we have further restricted the dataset to data that has an ARTIST quality control score of 90 or greater and to data that has been manually scaled. This quality control has resulted in a dataset of just over 6.2 million profiles. The stations used in constructing this dataset are represented in Figure 1.

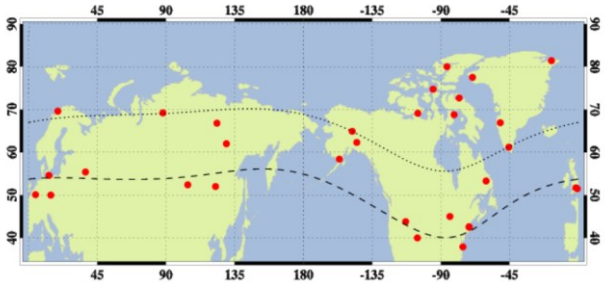

Figure 1. A map of the ionosonde stations used for the development of the bottomside portion of the E-CHAIM model.

As one will note, the dataset has significant holes, particularly over central Canada and over the Arctic Ocean. To deal with this issue, the bottomside portion of our model will be constructed in a magnetic latitude and magnetic local time coordinate system. In this way, we essentially "fill in" these data gaps by allowing each station to constrain the model along a zonal line at its magnetic latitude. Using such a coordinate system reduces the model's capability to reproduce geographically-dependent structures, such as non-migrating tides, but this is an unfortunate necessary compromise, which has been used in the past for the IRI's current hmF2 model [Altadill et al., 2009].

4. Bottomside Function

To define the shape of the bottomside electron density profile within E-CHAIM, we have chosen to create our own, unique, formulation. Unlike the data used in creating the IRI and NeQuick, we are making use of ionosonde data that does not explicitly provide profile parameters and instead simply directly provides the electron density profile. This makes us somewhat less confined to the use of the traditional method of using the F1-layer/ledge and E-region densities as anchor points for our profile function. In our formulation, we model the bottomside as a single semi-Epstein layer with an altitude-varying scale height. The functions used to define this scale height are themselves taken as a sum of semi-Epstein layers given below.

$$N(h) = \operatorname{sech}^2 z = \frac{4 \cdot NmF2}{(1+\exp(z))^2}\exp(z) \quad (1)$$

$$z = \frac{h - hmF2}{H} \quad (2)$$

$$H' = H_{F2} + H_{F1}\left[\operatorname{sech}^2\left(\frac{h-hmF1}{30.0}\right)\right] + H_E\left[\operatorname{sech}^2\left(\frac{h-hmE}{60.0}\right)\right] \quad (3)$$

$$H = H' \cdot \left[\frac{1}{1+\exp\left(\frac{hmE - 25.0 - h}{10.0}\right)}\right] \quad (4)$$

where H_{F2}, H_{F1}, and H_E are amplitude terms, H' is an intermediate scale height function, and H is the true scale height used by the model. You will note that the scale height function of Equation 3 is composed of two semi-Epstein layer functions, centered at hmF1 and hmE, with predefined thicknesses. These thicknesses were determined by optimizing RMS fitting error against a set of test thickness values. In Equation 4, we arrive at the true scale height, where the scale height function of Equation 3 is multiplied by a sigmoid function. This sigmoid function acts to suppress the scale height below the E-region, ensuring that the electron density tends to zero at the model's lower boundary.

This parameterization requires that we model hmF1, hmE, H_{F2}, H_{F1}, and H_E.

5. hmE and hmF1

We have chosen to independently develop models for hmE and hmF1. Beginning with hmE, we attempted to fit our dataset of ionosonde-derived hmE values to a model similar to that done for E-CHAIM's topside thickness. In so doing, we found RMS fitting errors hardly 0.5km improved over the standard deviation of the input data. This implies that even the most sophisticated modeling approach would only amount to a marginal improvement over simply using the average of the input data (102.19 ± 5.02 km). Based on this result, we have decided to simply use this average value in place of an explicit model for hmE. It is interesting here to note that both the IRI and NeQuick use constant values for hmE in their model; however, while the IRI's value of 105 km falls within the error range of the average derived here, the NeQuick's value of 120 km is substantially higher than the average by several standard deviations. This result may suggest a need to re-visit the NeQuick's choice of hmE.

Unlike hmE, hmF1 demonstrated notable coherent variability, such that a model could provide a substantial improvement over the mean (175.31 ± 15.01km). For hmF1, we have used a similar framework to that used for the topside thickness. The full parameterization is given as

$$hmF1 = G + \sum_{l=0}^{L}\sum_{m=0}^{\min(l,M)} F_1\left[A_{lm}\cos\left(\frac{\pi m}{180}MLT\right) + B_{lm}\sin\left(\frac{\pi m}{180}MLT\right)\right]P_{lm}(\eta) \quad (5)$$

$$C_{lm}, D_{lm} = \sum_{c=1}^{3}\alpha_{lm}^{c}\cos\left(\frac{2\pi c\cdot DoY}{365.25}\right) + \beta_{lm}^{c}\sin\left(\frac{2\pi c\cdot DoY}{365.25}\right) \quad (6)$$

$$\begin{aligned} G = {} & a_1\cos(\chi) + a_2\sin(\chi) + a_3\chi + a_4\chi^2 + a_5\chi^3 \\ & + \sin(\chi)\cdot(a_6\sin\theta + a_7\cos\theta) \\ & + \cos(\chi)\cdot(a_8\sin\theta + a_9\cos\theta) \\ & + a_{10}\sin\theta + a_{11}\cos\theta \\ & + AE'(a_{12}\sin\varphi + a_{13}\cos\varphi) \end{aligned} \quad (7)$$

where *F1* is 81-day smoothed F10.7 flux, *F2* is integrated AE index, *DoY* is the day of year, θ is the dipole tilt angle, χ is the solar zenith angle, $a_{1\text{-}12}$, α_{lm}^{c}, and β_{lm}^{c} are fitting coefficients, and η is the colatitude scaled to a 45° cap, described in Themens et al. [2017].

To assess the validity of the E-CHAIM hmF1 model fit, we present a comparison between hmF1 derived from E-CHAIM, the NeQuick parameterization (using measured hmF2), and the "traditional" hmF1 parameterization [Bilitza, 1990], currently used by ICEPAC, which parameterizes hmF1 as a linear function of solar zenith angle. A comparison of the median behaviour of hmF2 from these various models is presented in Figure 2. To illustrate the best possible representation based solely on solar zenith angle, we have also included a best fit to a quadratic function in solar zenith angle.

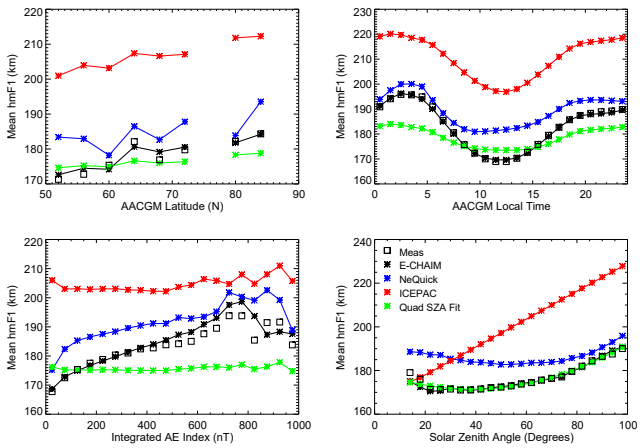

Figure 2. Plot of mean hmF1 behaviour vs. AACGM latitude (top left), AACGM local time (top right), integrated AE index (bottom left), and solar zenith angle (bottom right).

Examining first the patterns with respect to solar zenith angle, we see that the E-CHAIM and quadratic model fit the dataset's solar zenith angle behaviour very well. Also evident is the apparent inability of a linear parameterization in solar zenith angle to represent the behaviour of hmF1, which appears to be largely unchanged except at large solar zenith angles. The NeQuick appears to perform well when the sun is low to the horizon but poorly during mid-day. In terms of latitude, the ionosonde data demonstrates a largely linear trend with hmF1 increasing toward the geomagnetic pole. This pattern is well captured by the E-CHAIM fit. The best fitted quadratic model seems to underestimate the rate of increase with latitude, while both the NeQuick and the "traditional" parameterization are biased upward by ~8km and ~30km, respectively. In local time E-CHAIM and the ionosonde data demonstrate a local minimum at local noon and an asymmetric diurnal variation with higher morning hmF1 compared to the evening. As for the remaining models, the traditional approach appears to again be over estimating hmF1 by ~30km and the NeQuick model, while performing well at in the morning and evening, overestimates hmF1 around local noon. Interestingly, we see here that the best fitted solar zenith angle curve underestimates the amplitude of the diurnal variation of the and performs better during daytime periods than during the evening and morning periods, likely because of the abundance of daytime day as compared to morning and evening data (fit heavily weighted toward local noon). The inability of this function to capture the diurnal variation of hmF1, suggests that hmF1 may have a significant dependence on neutral composition behaviour, which may not simply follow a solar illumination-driven pattern. Finally, and perhaps most interesting, is the observed behaviour with respect to integrated AE index. Here we note a sudden increase in hmF1 from very quiet periods to more average periods with largely linear behaviour thereafter. Interestingly, the hmF2 parameterization of the NeQuick seems to capture the trend with respect to AE index reasonably well if one ignores the slight tendency for an upward bias. In fact, if one uses 105km for hmE, in place of the NeQuick's 120km value, we see average AE index behaviour comparable to that of the E-CHAIM model. This is also true for the latitudinal behaviour of the NeQuick's parameterization. This suggests that hmF2 may be a good target parameter when attempting to model hmF1. It should be noted, however, that we have used measured hmF2 here, and thus the CCIR-based hmF2 of the NeQuick would not capture such variabilities, as it does not include a geomagnetic activity adjustment.

Table 1 RMS errors from each hmF1 modeling method tested.

Method	RMS Error (km)
Mean	15.01
E-CHAIM	9.47
NeQuick	17.89
NeQuick (hmE = 105km)	15.48
Traditional Model	32.32
SZA Quadratic Fit	14.43

Overall RMS errors from each method are listed in Table 1. One will note from this table that the RMS error of the

traditional approach is significantly worse than the use of a constant mean value for hmF1 and that the NeQuick, using 120km for hmE also performs worse than a simple mean. In fact, if one used CCIR-derived hmF2 in the NeQuick parameterization, it can be presumed that these errors might have been much larger, given the errors in the IRI/NeQuick hmF2 presented in Themens et al. [2014]. Overall, the E-CHAIM fit performs substantially better than the mean and the NeQuick. It also performs much better than functions that are based solely on solar zenith angle.

6. Amplitudes: H_{F2}, H_{F1}, and H_E

With the hmE and hmF1 parameterizations completed, we then began fitting electron density profiles for the amplitude terms of Equation 3. This is done via nonlinear least squares with pre-specified values for the heights and thicknesses of the scale height layers. Ionosonde inversion errors are used to create a diagonalized measurement error covariance, the a priori covariances are also diagonalized, and all output amplitude values are constrained to be greater than zero. Examples of these fits to ionosonde-derived electron density profiles is provided in Figure 3.

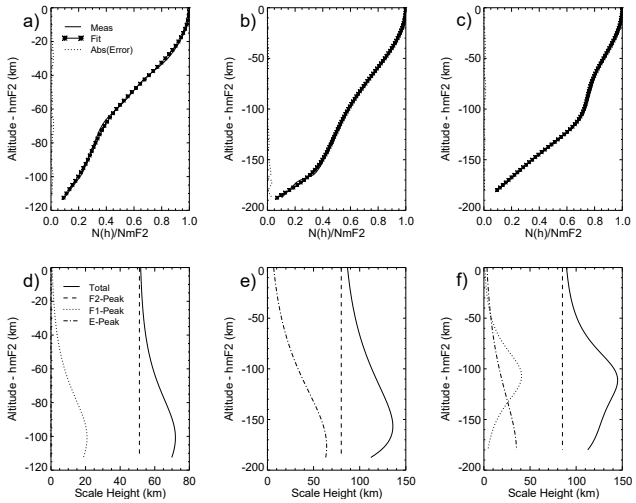

Figure 3 Example ionosonde-derived electron density profiles at Cambridge Bay (a-c) and corresponding scale height profiles (d-e) for three situations: a,d) no E-region trace, b,e) no F1-layer/ledge trace, and c,f) a profile with all three layers present. d-f) also demonstrate the various components of the scale height function.

As you may note, our chosen profile function does an excellent job fitting ionosonde-derived electron density profiles under a robust set of conditions. That said, there are an enormous number of profile functions that will fit an electron density profile. The challenge is finding one that produces physically consistent parameter variability that can be easily fitted to a model. For example, we attempted to use a fourth order polynomial to represent the scale height in our model; however, multiple attractors and the fact that none of the parameters of the fit were tied to a physical phenomenon meant that the fitted parameters did not exhibit coherent variability that could be easily fitted to a model. Our approach, of course, is not without some caveats: the various layers will often overlap, causing unwanted correlations between the layer amplitudes. To rectify this issue, we take a page out of the NeQuick's book by choosing to model the total scale height at each peak location instead of the amplitudes of each function. This results in modeling the following

$$\gamma = H_{F2} + H_{F1} f_{F1}(hmF2) + H_E f_E(hmF2) \quad (8)$$

$$\beta = H_{F2} + H_{F1} + H_E f_E(hmF1) \quad (9)$$

$$\alpha = H_{F2} + H_E + H_{F1} f_{F1}(hmE) \quad (10)$$

where f_E and f_{F1} are the semi-Epstein layer functions without their amplitude terms. Once these parameters are modeled, they are converted back into the function amplitudes using a simple rearranging of Equations 8-10.

These peak total scale heights will be modeled using the same spherical cap harmonic and Fourier expansion as that used for hmF1. The results of this fit will be presented in the associated presentation.

7. Conclusions

We have here presented the framework used to profile the bottomside of the E-CHAIM model. For this purpose, we have chosen to use a single semi-Epstein layer function with a varying scale thickness, whose coefficients (hmE, hmF1, and the amplitudes of the three layer functions) are modeled by a spherical cap harmonic and Fourier expansion. For hmE, we find that a constant value of 102 km is sufficient to properly represent the E-region altitude, while a more complicated spherical cap harmonic and Fourier expansion model of hmF1 shows significant improvement over other hmF1 models.

6. Acknowledgements

We'd like to thank all of the ionosonde operators that contribute to GIRO and the operators of GIRO for their contribution of data toward this project.

7. References

D. Bilitza (1990), International Reference Ionosphere 1990, NSSDC 90-22, Greenbelt, Maryland.

Bilitza, D. (2003). International Reference Ionosphere 2000: Examples of improvements and new features. *Adv. Space Res.*, 31(3), pp. 757-767.

Themens, D. R., P. T. Jayachandran, M. J. Nicolls, and J. W. MacDougall (2014), A top to bottom evaluation of IRI 2007 within the polar cap, *J. Geophys. Res. Space Physics*, **119**, 6689–6703, doi:10.1002/2014JA020052.

Themens, D.R., P.T. Jayachandran, I. Galkin, and C. Hall (2017). The Empirical Canadian High Arctic Ionospheric Model (E-CHAIM): NmF2 and hmF2, *J. Geophys. Res. Space Physics*, doi: 10.1002/2017JA024398

Reinisch, B., and X. Huang (2000), Redefining the IRI F1 Layer profile, Adv. Space Res., 25(l), 81-88.

Scotto, C., S. M. Radicella, and B. Zolesi (1998), An improved probability function to predict the F1 layer occurrence and L condition, Radio Sci., 33(6), 1763–1765, doi:10.1029/98RS02637.